Using Ambient Ion Beams to Write Nanostructured Patterns for Surface Enhanced Raman Spectroscopy**

Anyin Li,* Zane Baird, Soumabha Bag, Depanjan Sarkar, Anupama Prabhath, Thalappil Pradeep,* and R. Graham Cooks*

Abstract: *Electrolytic spray deposition was used to pattern surfaces with 2D metallic nanostructures. Spots that contain silver nanoparticles (AgNP) were created by landing solvated silver ions at desired locations using electrically floated masks to focus the metal ions to an area as little as 20 μm in diameter. The AgNPs formed are unprotected and their aggregates can be used for surface-enhanced Raman spectroscopy (SERS). The morphology and SERS activity of the NP structures were controlled by the surface coverage of landed silver ions. The NP structures created could be used as substrates onto which SERS samples were deposited or prepared directly on top of predeposited samples of interest. The evenly distributed hot spots in the micron-sized aggregates had an average SERS enhancement factor of 10^8. The surfaces showed SERS activity when using lasers of different wavelengths (532, 633, and 785 nm) and were stable in air.*

Metallic nanoparticles have attractive properties in catalysis, photonics, and chemical sensing.[1] Raman spectroscopy is a powerful nondestructive technique,[2] the sensitivity of which can be significantly improved through surface-enhanced or tip-enhanced methods.[3] The enhancement arises from the proximity of the analytes to intense localized fields created by nanoscale objects.[4] The capability to modify, coat, and pattern surfaces with nanostructures is important for SERS and also for a wider range of nanomaterials applications.[5] Conventionally, modified surfaces are constructed by delivering intact nanoparticles to target locations through dropcasting or spin coating.[6] However, the difficulty

in positioning discrete particles with control over orientation, position, and degree of aggregation means that drop casting of nanoparticles has not been widely used in the high-throughput preparation of SERS substrates. Immobilized and shell-isolated nanosystems[5b,6c,7] address these issues, but the necessary vacuum preparation procedures significantly increase the complexity of such approaches.

Ion/surface collisions including ion soft-landing have been used to fabricate surface structures under vacuum.[8] Recently an electrolytic spray ionization method[9] has been developed that is capable of generating noble metal ions directly from their solids under ambient conditions as precursors for nanoparticle synthesis. Herein, we report the in situ fabrication of SERS-active spots and micro-scale patterns by landing ionized silver at desired locations where spontaneous cathodic reduction takes place, allowing the creation of nanostructure assemblies.

Silver is a widely used SERS material[10] and the plasmon resonance of silver nanostructures is tunable through the visible to mid-infrared regions of the electromagnetic spectrum.[11] Electrolytic spray deposition readily creates spots of approximately 3 mm in diameter composed of silver particles (AgNP) at desired locations, both on top of previously deposited analyte as well as prior to analyte deposition (Figure 1). Both the NP-on-top and the NP-below config-
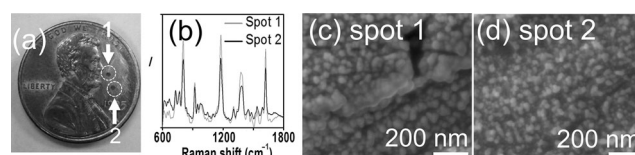

Figure 1. a) Two AgNP-containing spots created on a penny coin by electrolytic spray ionization deposition under ambient conditions. The top spot was created before drop casting a crystal violet sample ("NP-below") while the lower spot was created on top of a layer of crystal violet ("NP-on-top"). 10 Monolayers (ML) of silver ions were landed to create both spots, which showed similar morphology (c, d) and enhanced Raman signals (b).

urations prepared in this way showed uniformly distributed silver NPs in SEM images (Figure 1c,d). The particles were polydispersed in size and shape, yet the morphology was uniform across each spot (Figure 2, and Figures S4–S7 in the Supporting Information). On the one hand, the polydispersity conferred surface plasmon resonance activity over a wide energy range, making the spots SERS-active when using lasers of different wavelengths (532, 633, and 785 nm) in the cases of crystal violet and Rhodamine 6G as probe molecules

[*] Dr. A. Li, Z. Baird, Dr. S. Bag, Prof. R. G. Cooks
Department of Chemistry and Center for Advanced Analytical
Instrumentation Development, Purdue University
560 Oval Drive, West Lafayette, IN 47907 (USA)
E-mail: li273@purdue.edu
cooks@purdue.edu

D. Sarkar, A. Prabhath, Prof. T. Pradeep
DST Unit of Nanoscience (DST UNS) and Thematic Unit of
Excellence (TUE), Department of Chemistry, Indian Institute of
Technology Madras (IITM)
Chennai, 600 036 (India)
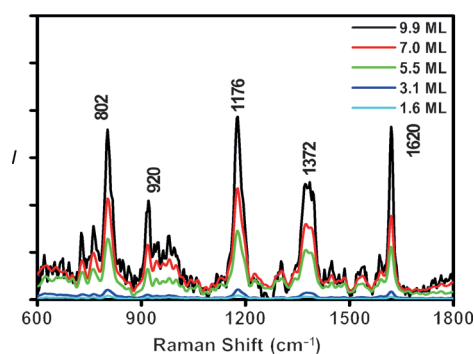E-mail: pradeep@iitm.ac.in

Figure 2. Effect of Ag coverage on SERS signal intensity from copper foil surface. See Figure S4 for the SEM images of the corresponding surfaces. Crystal violet ($\approx 10^5$ molecules per μm^2) was applied over the whole Ag deposition region by dropcasting. Each spectrum was acquired using 8.6 mW 633 nm laser excitation, with an acquisition time of 1 s.

(Figures S1 and S2). A resonance effect is evident using a 532 nm laser, but is avoided by using a 785 nm laser or by using R6G with a 633 nm laser. On the other hand, the uniform NP distribution resulted in numerous evenly distributed hot spots within each nanoparticle assembly (Figure S3). The robustness of this SERS surface is greatly enhanced by these features. Note that both the NP-on-top and the NP-below surfaces showed similar SERS enhancements, (Figure 1b).

Uniform spatial distribution of the landed silver ions (10 nA)[9] is critical for highly active surfaces. With the emitter tip (1–5 μm diameter) placed 5 mm from the cm-sized target, a roughly uniform charge distribution is created in the 2–5 mm diameter droplet plume, as mapped using a CCD atmospheric pressure ion detector (Figure S8).[12] The approximate uniformity in the central region of the spray was evident when examining the prepared structures using optical and electron microscopy. Coverage values were calculated from the accurately measured spot sizes and the logged deposition currents. The uniform SERS activity is most readily seen in Raman images (Figure S3a).

Using a copper foil as the support material, a coverage dependent study of the SERS enhancement was performed. As shown in Figure 2, the Raman signal for crystal violet (1 μM in MeOH, 2 μL dropcast to an approximately 3 mm spot) increased more than 10 times as the silver coverage increased from 1.6 ML to 5.5 ML and continued to increase until the CCD detector began to saturate at 9.9 ML when the average enhancement factor was 4×10^8.

SEM images for these surfaces (Figure S4) show single nanoparticles and a small number of aggregates at low surface coverage (1–3 ML). As the silver coverage was increased to 9.9 ML, the granules/particles grew larger and then aggregated with neighboring particles. This coverage-controlled in situ fabrication method produced uncapped NP structures. An important phenomenon is that features of the individual NPs were maintained during this aggregation process, creating numerous 1–5 nm gaps and crevices across the surface. This might be due to the fact that the particles were anchored to the metal surfaces during their growth. The nanojunctions and nanogaps (Figures S4 and S5d) observed are believed to

be ideal for creating SERS hot spots,[10,13] although the stability of the surfaces in air is more noteworthy. The SERS peak intensities are summarized in Tables S1 and S2. The enhancement factors (Table S2) were calculated using a previously reported method (see the Supporting Information, Section 2).[7,14]

For a circular landing spot of 3 mm diameter, the 10 nA ion current is equivalent to 0.03 ML/minute. At this rate, it took 5 h to prepare a 10 ML spot. A higher landing current density was achieved by positioning the emitter closer to the surface or by increasing the spray voltage from 1.5 kV to around 2.5 kV, which also increased the fluctuation of both landing current and spot size. By placing a mask of non-conductive material (or electrically floated conductive material) on top of the deposition surface, the landing current density was increased reproducibly (see the Supporting Information, Section 5). The local electric field that produced a focusing effect is generated by charge buildup on the mask material during ion deposition.[15] The simplest form of this idea was realized by applying a perforated plastic foil, or electrically floated metal mesh, on top of the deposition target, as shown for one particular experiment (Figure 3).
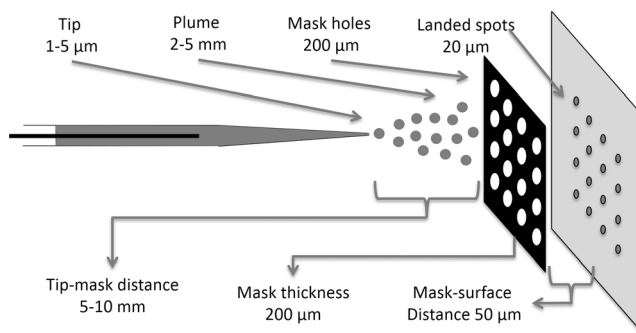

Figure 3. Schematic of the ionization, focusing, and deposition experiment. The drawing is not to scale, but the important dimensions (diameters and distances) are labelled. As a result of the charge-induced focusing effect, the spot sizes in the deposited patterns are 10 times smaller than those in the mask.

In typical experiments, this focusing effect increased the landing current density by a factor of around nine, with a 5–25% decrease in total ion current. Arrays of AgNP-containing spots were created in a single deposition process, simply by using masks with an array of apertures (Figure 3, and Figures S9–11).

The operations just described are essentially lithographic approaches similar to stencil vapor deposition in vacuum.[16] Under ambient conditions, ion beams and charged droplets manipulated by electric fields, magnetic fields, and pneumatic forces,[17] should be useful in lithography applications. Beyond static patterns, a coupled moving stage allowed writing of more detailed subpatterns (Figure 4).

Aside from the other applications inherent in these 2D structures,[18] these patterns are easily identifiable under microscopes and the patterned images also help to distinguish the synthesized nanoparticles from adventitious particles inevitably present in ambient experiments.
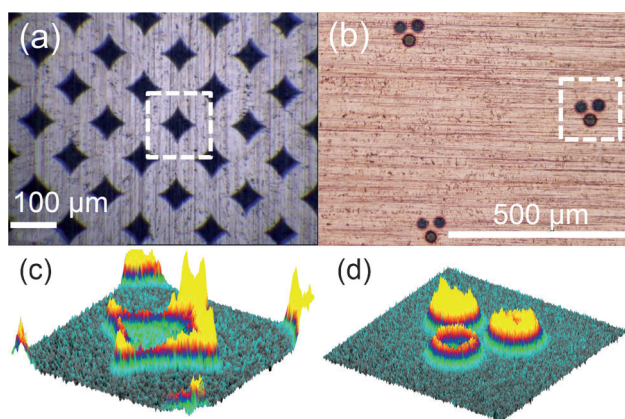
Figure 4. Optical images of a) AgNP patterns created using a grounded TEM grid as a static mask, and b) AgNP patterns created using a floated metal mesh as a mask while moving the copper target discontinuously underneath it. The movement created three-spot patterns visible at a number of locations. Images (c) and (d) are Raman maps of the selected (150×150 μm^2) regions in (a) and (b), respectively. Raman signals of the dropcast (≈3 mm diameter circle) crystal violet sample are only observable in the AgNP regions. The Raman intensity in the 1154 to 1204 cm^{-1} range was used for imaging. The highest peaks in the images correspond to a Raman signal (1176 cm^{-1} peak) of 41870 counts s$^{-1}\cdot$mw^{-1} in (c), and 37690 counts s$^{-1}\cdot$mw^{-1} in (d).

The choice of support material was also found to significantly influence the SERS activity of the deposited silver nanostructures, as is the case for other modification methods.[7,10,19] Generally, flat-polished slide supports gave much lower SERS enhancement factors under the same conditions (≈10 ML Ag coverage, Table S2). Copper, aluminum, and gold foils (not flat at the microscale) gave the highest average SERS enhancement factors (exceeding 10^7 and reaching 10^9), while brass and stainless steel foils gave weak enhancements. Although detailed mechanisms are not clear, the results for a gold foil support demonstrate that displacement plating[20] and oxide participation is not critical to the generation of SERS active surfaces by the electrospray deposition method. The flexible foils used here serve as efficient SERS sampling media, allowing dropcasting, wiping, spin coating, and spray deposition of samples. More importantly, samples can be present on the surface and hot spots can be generated in situ by depositing silver ions onto the sample spot (NP-on-top). Enhanced Raman signals were observed for all these methods.

In conclusion, the fabrication of nanostructures through electrolytic spray deposition is a "green", one-pot preparation method at ambient conditions that eliminates vacuum, lasers, and solution procedures associated with conventional nanofabrication. Micrometer-scale patterns can easily be made for SERS imaging and other purposes. Only sub-nanogram amounts of silver are consumed for each SERS substrate, spectra can be recorded in under a second, and the surfaces are stable in air for days. The enhancement factor is not unusual, but the simplicity of the fabrication method and the stability of the surfaces are noteworthy. Operation under atmospheric pressure further increases the ease of nanoscale surface modification. Electrolytic spray ionization deposition may serve well as a complement to sputtering or vapor deposition in other applications, such as the generation of plasmonic superstructures, catalysts, and in lithography.

[1] a) S. Eustis, M. A. El-Sayed, *Chem. Soc. Rev.* **2006**, *35*, 209–217; b) N. L. Rosi, C. A. Mirkin, *Chem. Rev.* **2005**, *105*, 1547–1562; c) P. K. Jain, X. H. Huang, I. H. El-Sayed, M. A. El-Sayed, *Acc. Chem. Res.* **2008**, *41*, 1578–1586.

[2] a) J. D. Biggs, Y. Zhang, D. Healion, S. Mukamel, *J. Chem. Phys.* **2012**, *136*, 174117; b) K. Kneipp, H. Kneipp, I, I, R. R. Dasari, M. S. Feld, *Chem. Rev.* **1999**, *99*, 2957–2976.

[3] a) D. L. Jeanmaire, R. P. Van Duyne, *J. Electroanal. Chem. Interfacial Electrochem.* **1977**, *84*, 1–20; b) H. Wang, Z. D. Schultz, *Analyst* **2013**, *138*, 3150–3157; c) R. M. Stockle, Y. D. Suh, V. Deckert, R. Zenobi, *Chem. Phys. Lett.* **2000**, *318*, 131–136.

[4] a) E. Hao, G. C. Schatz, *J. Chem. Phys.* **2004**, *120*, 357–366; b) D. A. Genov, A. K. Sarychev, V. M. Shalaev, A. Wei, *Nano Lett.* **2004**, *4*, 153–158; c) P. Negri, R. J. Flaherty, O. O. Dada, Z. D. Schultz, *Chem. Commun.* **2014**, *50*, 2707–2710.

[5] a) T. T. Nge, M. Nogi, K. Suganuma, *J. Mater. Chem. C* **2013**, *1*, 5235–5243; b) J. F. Li, Y. F. Huang, Y. Ding, Z. L. Yang, S. B. Li, X. S. Zhou, F. R. Fan, W. Zhang, Z. Y. Zhou, D. Y. Wu, B. Ren, Z. L. Wang, Z. Q. Tian, *Nature* **2010**, *464*, 392–395; c) J. Wang, L. Yang, B. Liu, H. Jiang, R. Liu, J. Yang, G. Han, Q. Mei, Z. Zhang, *Anal. Chem.* **2014**, *86*, 3338–3345.

[6] a) Y. N. Xia, J. A. Rogers, K. E. Paul, G. M. Whitesides, *Chem. Rev.* **1999**, *99*, 1823–1848; b) D. R. Baer, M. H. Engelhard, G. E. Johnson, J. Laskin, J. F. Lai, K. Mueller, P. Munusamy, S. Thevuthasan, H. F. Wang, N. Washton, A. Elder, B. L. Baisch, A. Karakoti, S. V. N. T. Kuchibhatla, D. Moon, *J. Vac. Sci. Technol. A* **2013**, *31*, 050820; c) K. D. Osberg, M. Rycenga, G. R. Bourret, K. A. Brown, C. A. Mirkin, *Adv. Mater.* **2012**, *24*, 6065–6070; d) J. Cyriac, M. Wleklinski, G. T. Li, L. Gao, R. G. Cooks, *Analyst* **2012**, *137*, 1363–1369.

[7] N. G. Greeneltch, M. G. Blaber, A. I. Henry, G. C. Schatz, R. P. Van Duyne, *Anal. Chem.* **2013**, *85*, 2297–2303.

[8] a) S. Rauschenbach, F. L. Stadler, E. Lunedei, N. Malinowski, S. Koltsov, G. Costantini, K. Kern, *Small* **2006**, *2*, 540–547; b) G. E. Johnson, T. Priest, J. Laskin, *J. Phys. Chem. C* **2012**, *116*, 24977–24986; c) Y. Lei, F. Mehmood, S. Lee, J. Greeley, B. Lee, S. Seifert, R. E. Winans, J. W. Elam, R. J. Meyer, P. C. Redfern, D. Teschner, R. Schlogl, M. J. Pellin, L. A. Curtiss, S. Vajda, *Science* **2010**, *328*, 224–228; d) J. Cyriac, T. Pradeep, H. Kang, R. Souda, R. G. Cooks, *Chem. Rev.* **2012**, *112*, 5356–5411; e) X. Li, K. A. Wepasnick, X. Tang, Y. Wang, K. H. Bowen, D. H. Fairbrother, G. Gantefoer, *J. Vac. Sci. Technol. B* **2012**, *30*, 031806.

[9] A. Li, Q. Luo, S.-J. Park, R. G. Cooks, *Angew. Chem. Int. Ed.* **2014**, *53*, 3147–3150; *Angew. Chem.* **2014**, *126*, 3211–3214.

[10] S. M. Asiala, Z. D. Schultz, *Analyst* **2011**, *136*, 4472–4479.

[11] T. R. Jensen, M. D. Malinsky, C. L. Haynes, R. P. Van Duyne, *J. Phys. Chem. B* **2000**, *104*, 10549–10556.

[12] O. Hadjar, G. Johnson, J. Laskin, G. Kibelka, S. Shill, K. Kuhn, C. Cameron, S. Kassan, *J. Am. Soc. Mass Spectrom.* **2011**, *22*, 612–623.

[13] Y. Fang, N. H. Seong, D. D. Dlott, *Science* **2008**, *321*, 388–392.

[14] I. Chakraborty, S. Bag, U. Landman, T. Pradeep, *J. Phys. Chem. Lett.* **2013**, *4*, 2769–2773.

[15] a) J. W. Kim, Y. Yamagata, B. J. Kim, T. Higuchi, *J. Micromech. Microeng.* **2009**, *19*, 025021; b) J. Ju, Y. Yamagata, T. Higuchi, *Adv. Mater.* **2009**, *21*, 4343–4347.

[16] J. C. Hulteen, R. P. Vanduyne, *J. Vac. Sci. Technol. A* **1995**, *13*, 1553–1558.

[17] a) A. K. Badu-Tawiah, A. Li, F. P. M. Jjunju, R. G. Cooks, *Angew. Chem. Int. Ed.* **2012**, *51*, 9417–9421; *Angew. Chem.* **2012**, *124*, 9551–9555; b) A. K. Badu-Tawiah, C. P. Wu, R. G.

Cooks, *Anal. Chem.* **2011**, *83*, 2648–2654; c) Z. Baird, W. P. Peng, R. G. Cooks, *Int. J. Mass Spectrom.* **2012**, *330*, 277–284.

[18] K. M. Evans-Nguyen, S. C. Tao, H. Zhu, R. J. Cotter, *Anal. Chem.* **2008**, *80*, 1448–1458.

[19] K. V. G. K. Murty, M. Venkataramanan, T. Pradeep, *Langmuir* **1998**, *14*, 5446–5456.

[20] a) X. M. Lu, H. Y. Tuan, J. Y. Chen, Z. Y. Li, B. A. Korgel, Y. N. Xia, *J. Am. Chem. Soc.* **2007**, *129*, 1733–1742; b) M. C. Liu, Y. Q. Zheng, L. Zhang, L. J. Guo, Y. N. Xia, *J. Am. Chem. Soc.* **2013**, *135*, 11752–11755.